^{18}F-FDG PET/MRI in Chronic Sciatica: Early Results Revealing Spinal and Nonspinal Abnormalities

Peter W. Cipriano*[1], Daehyun Yoon*[1], Harsh Gandhi[1], Dawn Holley[1], Dushyant Thakur[1], Brian A. Hargreaves[1], David J. Kennedy[2], Matthew W. Smuck[2], Ivan Cheng[2], and Sandip Biswal[1]

[1]Department of Radiology, Stanford University School of Medicine, Stanford, California; and [2]Department of Orthopaedics, Stanford University School of Medicine, Stanford, California

Chronic sciatica is a major cause of disability worldwide, but accurate diagnosis of the causative pathology remains challenging. In this report, the feasibility of an ^{18}F-FDG PET/MRI approach for improved diagnosis of chronic sciatica is presented. **Methods:** ^{18}F-FDG PET/MRI was performed on 9 chronic sciatica patients and 5 healthy volunteers (healthy controls). Region-of-interest analysis using SUV_{max} was performed, and ^{18}F-FDG uptake in lesions was compared with that in the corresponding areas in healthy controls. **Results:** Significantly increased ^{18}F-FDG uptake was observed in detected lesions in all patients and was correlated with pain symptoms. ^{18}F-FDG–avid lesions not only were found in impinged spinal nerves but also were associated with nonspinal causes of pain, such as facet joint degeneration, pars defect, or presumed scar neuroma. **Conclusion:** The feasibility of ^{18}F-FDG PET/MRI for diagnosing pain generators in chronic sciatica was demonstrated, revealing various possible etiologies.

Key Words: ^{18}F-FDG; PET/MRI; sciatica; pain

J Nucl Med 2018; 59:967–972
DOI: 10.2967/jnumed.117.198259

Sciatica is pain radiating from the buttock or lower back downward along the sciatic nerve into 1 leg or, less frequently, both legs (*1*). The most common cause of sciatica is a herniated intervertebral disk impinging on a lumbar spinal nerve (*2*). However, a wide variety of other spinal and nonspinal causes have been implicated as the source of sciatica (*3–5*). Accordingly, determining the source of chronic sciatica with current diagnostic methods remains challenging. Sciatica becomes chronic in an estimated 20%–30% of patients with the disease (*6*), and invasive treatments may be required for pain relief. Therefore, accurate identification of the pain source is essential to guiding appropriate interventions.

No clinical test that offers both high sensitivity and high specificity for identifying the source of sciatica has been established (*7*). History taking and physical examination are routinely performed, but their function in identifying the source of pain is limited (*1,6*). Electromyography may identify muscular denervation and isolate the injury to a specific spinal nerve (*8*). However, electromyography requires painfully invasive needle electrode insertion, and the sampling and interpretation process can be biased by the practitioner's skills (*9*). Although MRI is currently the imaging modality of choice for sciatica diagnosis, its findings often do not correlate with symptoms. For example, abnormal disk morphology on MRI in patients with chronic sciatica can be indistinguishable from that in patients whose sciatica has resolved (*10*).

^{18}F-FDG PET/MRI is a novel diagnostic approach that can offer metabolic and structural examinations of painful lesions. Compared with separate acquisition with each modality, simultaneous acquisition with PET and MRI can greatly mitigate motion-induced misregistration. This advantage is significant for specifying pain sources because the common sources of sciatic pain, such as a herniated disk, degenerated facet joints, and impinged spinal nerves, are located very close to one another. The high sensitivity of ^{18}F-FDG PET for metabolically hyperactive foci can be used to detect an abnormal increase in metabolism caused by painful inflammation. A recent PET imaging study demonstrated increased ^{18}F-FDG uptake in injured nerves of rats as well as in denervated calf musculature of the affected limb (*11*). Unfortunately, the low spatial resolution and lack of tissue contrast of PET limit distinction among multiple possible pathologies for a detected lesion. The high-resolution anatomic views and superior soft-tissue contrast of MRI can help to resolve the anatomic ambiguity of PET (*12*). On the other hand, when multiple or subtle structural abnormalities are detected on MRI, the metabolic contrast on PET can highlight the pain-relevant inflammatory changes within the detected lesions.

The aim of this study was to investigate the feasibility of whole-body ^{18}F-FDG PET/MRI as a diagnostic tool for visualizing hypermetabolic and inflamed pathology in chronic sciatica. We performed whole-body ^{18}F-FDG PET/MRI on chronic sciatica patients and asymptomatic controls and compared the ^{18}F-FDG uptake patterns in these groups.

MATERIALS AND METHODS

Patient Population

The Stanford University Institutional Review Board approved our prospective observational study, and all subjects (both patients and controls) signed a written informed consent form. All data were collected in compliance with the Health Insurance Portability and Accountability Act. The clinical trial registration number of this study is NCT03195270. Nine patients presenting with chronic sciatica symptoms (unilateral leg pain greater than back pain for at least 3 mo) were recruited for the patient group (5 men and 4 women; mean age, 38.2 y [SD, 12.7 y]; age range, 21–58 y). At the time of imaging,

Received Jul. 15, 2017; revision accepted Oct. 23, 2017.
For correspondence or reprints contact: Sandip Biswal, 300 Pasteur Dr., S-068B, Stanford, CA 94305.
E-mail: biswal@stanford.edu
*Contributed equally to this work.
Published online Nov. 2, 2017.

all patients had a pain score of at least 4 on a 10-cm visual analog scale, where 0 cm was no pain and 10 cm was the worst pain imaginable. We also performed ^{18}F-FDG PET/MRI on 5 asymptomatic volunteers, who served as the control group (2 men and 3 women; mean age, 34.2 y [SD, 8.4 y]; age range, 22–48 y).

PET/MR Imaging Process

All subjects fasted for at least 4 h before the imaging session to ensure a blood glucose level below 180 mg/dL at the time of imaging. The mean administered activities of ^{18}F-FDG in patients and controls were 362.6 MBq (SD, 17.7 MBq; range, 327.7–380.5 MBq) and 359.5 MBq (SD, 26.7 MBq; range, 318.8–389.3 MBq), respectively. The mean administered activities normalized to body weight in patients and controls were 4.59 MBq/kg (SD, 0.63 MBq/kg; range, 4.38–6.08 MBq/kg) and 4.22 MBq/kg (SD, 1.13 MBq/kg; range, 3.75–6.58 MBq/kg), respectively. One hour after a single bolus injection of ^{18}F-FDG, subjects underwent PET/MRI in a GE PET/MRI scanner (SIGNA PET/MR; GE Healthcare). Subjects were scanned from the head to the feet in 8–10 bed positions for 1 to 1.5 h, depending on the height of the patient. PET images were reconstructed with product reconstruction software using MR-based attenuation correction techniques (*13–15*). A common color scale ranging from 0 to 3 for SUV was used to render all of the PET images.

The following MRI sequences were performed simultaneously with PET scans for each bed: 3-dimensional coronal double-echo steady-state (repetition time [TR], 18.7 ms; echo time [TE], 8.1 ms; resolution, 1.2 × 1.2 × 2 mm; flip angle, 30°), 3-dimensional axial liver imaging with volume acceleration-flexible (TR, 4.6 ms; TE, 1.8 ms; resolution, 1.3 × 1.3 × 3.4 mm; flip angle, 15°), 3-dimensional axial double-echo steady-state (TR, 18.3 ms; TE, 6.4 ms; resolution, 0.7 × 0.7 × 2 mm; flip angle, 30°), and 2-dimensional axial T2-weighted fast spin-echo with fat saturation (TR, 5 s; TE, 76 ms; resolution, 1 × 1 × 2 mm; echo train length, 8). For signal reception, a 16-channel head-neck coil, an integrated spine coil, and two 32-channel body phase-array coils were used.

Analysis of ^{18}F-FDG PET/MR Images

We performed image analysis to identify ^{18}F-FDG PET/MRI abnormalities by comparison with the contralateral side and with controls. We first conducted a radiologic review of PET/MR images from patients to detect the lesions likely causing their symptoms. Two radiologists performed the review to identify structural abnormalities on MRI or focal hot spots on PET. Hot spot detection was based on the asymmetry of the ^{18}F-FDG uptake or a qualitative comparison with the imaging pattern of controls. No patient information was used during the review to avoid any bias in the detection of abnormalities. Rigorously validating the pain relevance of detected abnormalities requires the direct treatment of those abnormalities and the evaluation of the pain relief outcome, which were beyond the scope of this research. In this study, we simply compared the side (left/right) of the reported pain with the side of the identified abnormalities.

To categorize lesions in the lumbar spine, we performed a region-of-interest analysis for ^{18}F-FDG uptake by segmenting the following 5 areas at each lumbar spine level (L1–L5) on the basis of coregistered MRI anatomy: disk, lateral recess, neuroforamen, facet joint, and paraspinal muscle. We used Osirix (version 8.0; Pixmeo SARL) for the image segmentation and SUV measurement. To establish baseline measurements of ^{18}F-FDG uptake, we calculated the mean and SD of the SUV_{max} in the same segmented areas of controls. For all detected lesions, both spinal and nonspinal, we measured the SUV_{max} and compared it with the contralateral SUV_{max}.

For lesions of spinal nerve impingement due to a herniated disk (the most common cause of sciatica), the SUV_{max} was obtained from the lesion itself, the equivalent location on the contralateral side, and the corresponding location in controls. These values were compared using the Mann–Whitney *U* test to determine statistical significance ($P < 0.01$).

RESULTS

MRI Abnormalities

Spinal nerve impingement due to a herniated disk was detected in 6 of 9 patients, and in none was the nerve impingement bidirectional, as summarized in Table 1. Impingement occurred at the L5–S1 vertebral level in all but 1 case, in which impingement occurred at the L4–L5 level. In the remaining 3 patients, bilateral L5 pars defects with L4–S1 spinal nerve neuritis, S2 peripheral nerve entrapment by the piriformis muscle, and bilateral L5–S1 facet arthropathy were identified.

^{18}F-FDG Uptake in Lumbar Spine of Asymptomatic Controls

The ^{18}F-FDG SUV_{max} (mean and SD) in segmented tissues at different levels of the lumbar spine in the 5 controls is shown in Table 2. The average SUV_{max} in the neuroforamen and facet joints was generally between 1.0 and 1.2. The average SUV_{max} in the disk, lateral recess, and paraspinal muscle were mostly distributed between 0.6 and 0.8. These values served as a baseline in the visual recognition of ^{18}F-FDG hot spots in patients during the radiologic review.

^{18}F-FDG PET Abnormalities

Focally increased ^{18}F-FDG uptake was found in both spinal and nonspinal tissues, as shown in Table 1. In patients 1–5, an abnormally high SUV_{max} (ranging from 1.26 to 1.75) was identified in the lateral recess—at the L5–S1 level in patients 1–3 and 5 and at the L4–L5 level in patient 4. The coregistration of MRI revealed that the lateral recess was narrowed because of disk herniation. In all cases, the SUV_{max} in these lesions was higher than the SUV_{max} on the contralateral side, as shown in Figure 1A. The difference in the SUV_{max} between the 2 sides was the smallest in patient 3, in whom subtle compression of the contralateral spinal nerve was also observed. The SUV_{max} in lesions and the SUV_{max} on the contralateral sides in patients were higher than the mean SUV_{max} in controls (green dotted line in Fig. 1A). Because the lesions revealed by PET/MRI were found at the L4–S1 levels, the mean SUV_{max} in controls was calculated at the same levels.

Figure 1B shows the distributions of the SUV_{max} in Figure 1A. The *P* values from the Mann–Whitney *U* test of the SUV_{max} in lesions against the SUV_{max} on the contralateral sides and in controls were all less than 0.01, indicating a significant difference in their medians. Patients 1–5 also had high ^{18}F-FDG uptake in leg muscles, including the biceps femoris, extensor hallucis longus, soleus, and tibialis anterior muscles ipsilateral to the side of disk herniation. The SUV_{max} in these muscles ranged from 1.0 to 2.5—higher than the contralateral SUV_{max} by 15%–96%.

In patients 6–9, no high ^{18}F-FDG uptake was detected in the lateral recesses of the lumbar spine. Instead, the ^{18}F-FDG uptake abnormalities were found in the following locations: the S2 peripheral nerve entrapped by the piriformis muscle (SUV_{max}, 1.4), a focal spot in the left calf muscles (SUV_{max}, 1.84), the left L5–S1 facet joint (SUV_{max}, 2.94), the left hamstring tendon (SUV_{max}, 2.1), and the L5 pars defect (SUV_{max}, 1.3). The SUV_{max} in these areas was higher than the contralateral SUV_{max} by 14%–54%.

Relevance of PET/MRI Abnormalities to Pain Symptoms

In patients 1–5, both MRI and ^{18}F-FDG PET showed abnormalities in the lateral recess on the side ipsilateral to the patient's pain symptoms. More specifically, asymmetrically high ^{18}F-FDG uptake colocalized to the herniated disk and the adjacent compressed spinal nerve was observed with MRI. These same 5 patients also had increased ^{18}F-FDG uptake in the leg ipsilateral

TABLE 1
Abnormal ^{18}F-FDG PET/MRI Findings for Patients

Patient	Painful side	Location	SUV_{max} of ^{18}F-FDG on: Lesion side	SUV_{max} of ^{18}F-FDG on: Contralateral side	MRI abnormalities
1	Right	Right L5–S1 lateral recess	1.66	1.08	Compression of right S1 spinal nerve by disk bulge at L5–S1
		Right biceps femoris muscle	1.39	0.85	
2	Right	Right L5–S1 lateral recess	1.34	1.05	Compression of right S1 spinal nerve by disk bulge at L5–S1
		Right biceps femoris muscle	1.00	0.51	
		Right extensor halluces longus muscle	2.50	1.33	
3	Right	Right L5–S1 lateral recess	1.26	1.18	Compression of right S1 spinal nerve by disk bulge at L5–S1
		Right biceps femoris muscle	1.42	1.24	
4	Left	Left L4–L5 lateral recess	1.36	1.06	Compression of left L5 spinal nerve by disk bulge at L4–L5
		Left soleus muscle	1.10	0.84	
5	Right	Right L5–S1 lateral recess	1.75	1.20	Compression of right S1 spinal nerve by disk bulge at L5–S1
		Right tibialis anterior muscle	1.24	0.82	
6	Right	Right S2 peripheral nerve	1.4	1.2	Entrapment of right S2 peripheral nerve by piriformis muscle
7	Left	Left gastrocnemius and soleus muscles	1.84	0.84	Mild compression of right S1 spinal nerve by disk bulge at L5–S1
8	Left	Left L5–S1 facet joint	2.94	1.53	Bilateral facet arthropathy at L5–S1
		Left hamstring tendon	2.1	1.4	
9	Left	Left L5 pars	1.30	0.80	Bilateral L5 pars defects; neuritis at left L4–S1 spinal nerve

to the site of symptoms, whereas the corresponding MRI of the same leg did not show any signal or structural abnormalities. Figure 2 depicts a representative case among these patients. The axial MR image shows the descending right S1 spinal nerve impinged by focal protrusion of the L5–S1 disk (yellow arrow in Fig. 2A) and an abnormally increased SUV_{max} (yellow arrow in Fig. 2C) compared with that on the contralateral side (1.66 vs. 1.08). The coronal MR image of both legs of the same patient shows no structural abnormalities (Fig. 2D). The coronal PET image, however, shows abnormal ^{18}F-FDG uptake in the biceps femoris muscle (red arrow in Fig. 2E). The SUV_{max} in this muscle was 1.39—much higher than the contralateral SUV_{max} (0.85) (Fig. 2F).

In patient 6, the MRI and PET abnormalities were detected in the same area ipsilateral to the patient's pain as well, but they were in nonspinal areas (S2 peripheral nerve).

TABLE 2
SUV_{max} in Lumbar Spine Areas of Controls

Location	SUV_{max} at: L1–L2 Mean	SD	L2–L3 Mean	SD	L3–L4 Mean	SD	L4–L5 Mean	SD	L5–S1 Mean	SD
Lateral recess	0.90	0.18	0.69	0.15	0.71	0.21	0.70	0.21	0.71	0.17
Neuroforamen	1.23	0.23	1.24	0.23	1.20	0.27	1.10	0.17	1.05	0.25
Disk	0.75	0.15	0.61	0.15	0.61	0.18	0.68	0.13	0.68	0.23
Facet joints	1.11	0.26	1.18	0.26	1.06	0.25	1.18	0.30	1.00	0.22
Paraspinal muscle	0.77	0.13	0.73	0.17	0.75	0.18	0.67	0.15	0.66	0.22

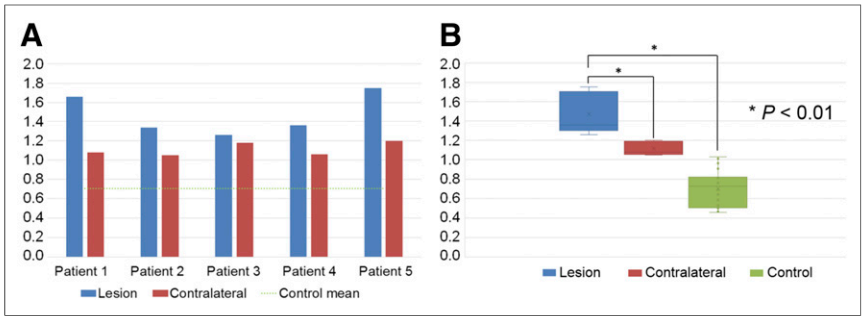

FIGURE 1. ^{18}F-FDG SUV_{max} in lateral recess in lesions, contralateral sides, and controls. (A) ^{18}F-FDG SUV_{max} in lesions of impinged spinal nerve due to herniated disk and contralateral SUV_{max} in 5 patients. Mean SUV_{max} in controls is plotted in green dotted line. (B) Distributions of ^{18}F-FDG SUV_{max} in lesions, contralateral sides, and controls in A. Mann–Whitney *U* test demonstrated *P* values of less than 0.01 in comparisons of SUV_{max} between lesions and contralateral sides and in comparisons of SUV_{max} between lesions and controls.

In patients 7–9, the MRI abnormalities were not always detected on the same side as the patient's pain symptoms. In patient 7, the MRI abnormalities were detected on the side opposite the patient's pain (Fig. 3). The MR image shows the impinged S1 spinal nerve in the right lateral recess (green arrow in Fig. 3A), but the patient's pain was on the left side. Interestingly, no significant ^{18}F-FDG uptake was observed in either lateral recess (Fig. 3B) or at any vertebral level of the lumbar spine. Although MRI of the lower extremities showed no structural abnormalities (Fig. 3C), a discrete focus of high ^{18}F-FDG uptake (SUV_{max}, 1.84) was found between the left gastrocnemius and soleus muscles (Fig. 3D). In this region of high ^{18}F-FDG uptake, the patient reported a superficial area of numbness. The corresponding location on the contralateral limb yielded a substantially lower SUV_{max} (0.84), and the patient did not report numbness in this area. The medical history of the patient revealed a direct traumatic blow to the region from a skiing accident. We suspect that the image abnormality was a scar neuroma that resulted from the accident and caused the local skin numbness and the leg pain.

In each of patients 8 and 9, the MRI abnormalities were detected bilaterally, whereas the PET abnormalities were detected only on the side ipsilateral to the pain. The axial MR image for patient 8 shows mildly hypertrophied and osteophytic facet joints bilaterally at the L5–S1 level (Fig. 4A). This MR finding was not convincing enough to ensure its contribution to the patient's symptoms. However, very significant ^{18}F-FDG uptake (SUV_{max}, 2.94) was observed around the left L5–S1 facet joint ipsilateral to the patient's pain (white arrows in Fig. 4B), boosting the likelihood of the left L5–S1 facet joint being the source of the pain rather than the right facet joint.

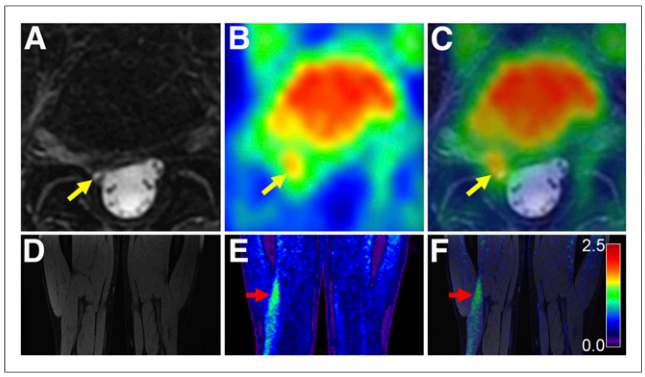

FIGURE 2. ^{18}F-FDG PET/MRI findings in patient with right-side sciatica and spinal nerve impingement due to herniated disk. (A) Axial T2-weighted fast spin-echo MR image showing herniated disk at L5–S1 level compressing descending S1 spinal nerve in right lateral recess (yellow arrow). (B) ^{18}F-FDG PET image showing asymmetrically increased ^{18}F-FDG uptake on right side. (C) ^{18}F-FDG PET/MRI coregistered image displaying increased uptake in impinged S1 spinal nerve (yellow arrow). (D) Coronal double-echo steady-state MR image of midthighs demonstrating no structural damage, such as muscle atrophy or muscle edema, from denervation. (E) ^{18}F-FDG PET image illustrating high ^{18}F-FDG uptake in right leg (red arrow). (F) ^{18}F-FDG PET/MRI coregistered image showing high ^{18}F-FDG uptake in biceps femoris muscle. For all PET images, common color scale ranging from 0.0 to 2.5 was used for SUV, as in color bar in F.

DISCUSSION

In this article, we presented ^{18}F-FDG PET/MRI findings for 9 chronic sciatica cases to demonstrate the feasibility of our ^{18}F-FDG PET/MRI approach for locating the source of sciatica. In 5 of 9 patients, spinal nerve impingement due to a herniated disk was identified as a relevant lesion on the basis of both MRI morphology and high ^{18}F-FDG uptake. In the remaining 4 patients, different types of lesions were found in the leg muscles, peripheral nerve, pars, and facet joints, where ^{18}F-FDG uptake was abnormally high but only mild abnormalities or no abnormalities appeared on MRI.

The complementary combination of the metabolic interrogation by ^{18}F-FDG PET and the anatomic localization by 3-T MRI showed potential for improved identification of the sciatic pain sources in a limited number of patients with sciatica. For example, the morphologic findings on MRI could contribute to specifying the type of lesion detected by PET for the spinal nerve root impingement case shown in Figure 1. The high ^{18}F-FDG uptake might indicate a potentially painful lesion but, in the absence of MRI, could not specify the type of lesion among possible local pathologies, such as tumor, facet synovitis, disk herniation, or other causes of an impinged spinal nerve. Coregistration of the PET and MR images specifically identified the lesion as spinal nerve impingement by a herniated disk. Our results also demonstrated (Fig. 3) that focal, increased ^{18}F-FDG uptake could help delineate pain-relevant pathology when multiple structural abnormalities were observed on MRI. The radiologic review of the MR image without the patient information suggested that the descending right S1 spinal nerve impingement might cause sciatic nerve pain on the right side. However, this finding was a false-positive one because the patient's pain was on the contralateral side. Evaluation of the ^{18}F-FDG PET/MR image demonstrated a lack of ^{18}F-FDG uptake in the protruding disk and impinged nerve, thus decreasing the importance of this MR finding.

The high ^{18}F-FDG uptake observed in the leg muscles without any structural abnormalities on MRI suggested a few possible etiologies for sciatica. First, the patient may actually have a herniated disk and nerve impingement. This injury to the nerve is

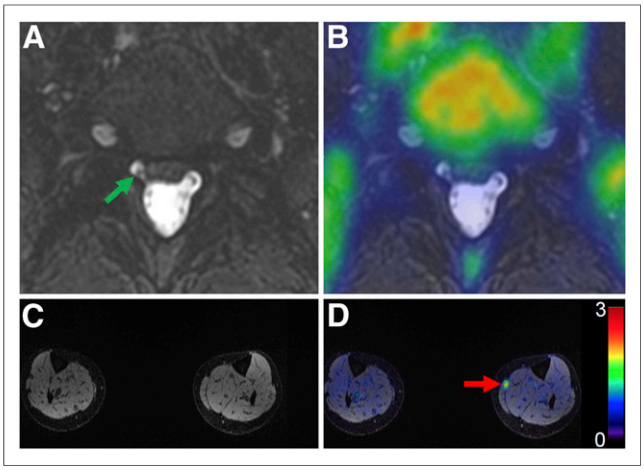

FIGURE 3. Different findings from ^{18}F-FDG PET and MRI in patient with left-side sciatica. (A) Axial T2-weighted fast spin-echo MR image indicating impingement of right S1 spinal nerve by herniated disk at L5–S1 level (green arrow). This finding is not likely to be cause of sciatica because pain is on other side. (B) ^{18}F-FDG PET/MRI coregistered image showing no asymmetrically increased ^{18}F-FDG uptake in impinged spinal nerve relative to contralateral side. (C) Axial double-echo steady-state MR image of lower leg (calf) revealing no structural degeneration or signal abnormalities. (D) ^{18}F-FDG PET/MRI coregistered image demonstrating high ^{18}F-FDG uptake in left gastrocnemius and soleus muscles (red arrow), where patient reported skin numbness.

known to give rise to downstream neuropathic changes in muscle, including edema or atrophy. A second possibility is that the abnormal ^{18}F-FDG uptake in the muscle may reflect a primary problem with the muscle (e.g., infectious or noninfectious myositis, ischemia, or trauma), mimicking the symptoms of spinal sciatica. In this case, a diagnostic local anesthetic injection to the focus of the high ^{18}F-FDG uptake in the muscle may be useful for confirming or refuting the peripheral pain source. A third possible reason for the abnormal muscular uptake of ^{18}F-FDG is that altered mechanics to accommodate or minimize painful conditions will result in the recruitment of muscles that are not necessarily pain generators (e.g., gait alteration or limp). We believe that a longitudinal study of a larger patient population is required to rigorously classify and validate these potential nonspinal sources of sciatica.

Our whole-body imaging approach allowed for the investigation of potential abnormalities in other body parts that might differentiate sciatica patients from asymptomatic controls. Although we observed both spinal and nonspinal manifestations of disease in sciatica patients, a more systematic search would be needed to determine the involvement of other body structures in the disease. For example, quantitative correlation of the ^{18}F-FDG PET/MRI patterns in the central nervous system with the symptoms and detected abnormalities in the lower extremities would be an interesting topic for future research.

In asymptomatic controls, we often observed a higher-than-background ^{18}F-FDG uptake pattern in the extensor compartment of both forearms (SUV_{max} ranging from 0.5 to 4.2). We suspect that this finding was due to mechanical recruitment of these muscles, either just before or during injection of the radiotracer, despite our efforts to keep patients in a relaxed position. Another common, nonspecific pattern in asymptomatic controls was high ^{18}F-FDG uptake in the anterior compartment muscles of the lower legs (SUV_{max} ranging from 0.5 to 3 in the anterior tibialis, extensor digitorum longus, and extensor hallucis longus muscles). We suspect that this finding was also due to mechanical recruitment of these muscles immediately before or during the injection of ^{18}F-FDG.

The present study was limited by the small size of the patient and control populations as well as potential selection bias because the patients had a chronic condition. Although the results are encouraging, our findings are based on the imaging results from only 9 sciatica patients and 5 asymptomatic controls. Therefore, an investigation with a larger cohort of patients should be performed to robustly determine the ^{18}F-FDG PET/MRI phenotypes of chronic sciatica. For future studies, MRI sequences could be customized to improve the value of MRI beyond anatomic investigation. For example, diffusion MRI techniques for the evaluation of spinal nerve compression (*16–18*) have shown promising results. Finally, monitoring the course of treatment for patients after our PET/MRI study can provide data for evaluating the predictive value of the imaging findings and their contributions to treatment options.

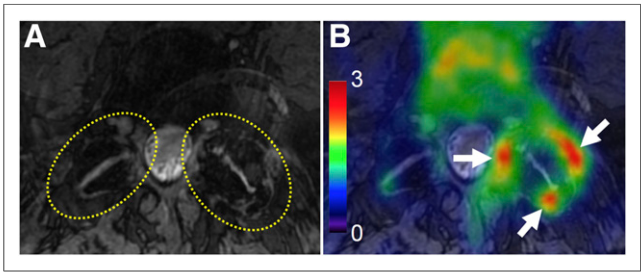

FIGURE 4. ^{18}F-FDG PET/MRI findings in patient with left-side sciatica and bilateral MRI abnormalities. (A) Axial double-echo steady-state MR image showing degenerated L5–S1 facet joints bilaterally, mild form of hypertrophy, and osteophyte (yellow dotted circles). (B) ^{18}F-FDG PET/MRI coregistered image revealing high ^{18}F-FDG uptake around degenerated L5–S1 facet joint on left side only (white arrows).

CONCLUSION

We presented a novel ^{18}F-FDG PET/MRI approach for diagnosing the source of chronic sciatica. Our approach demonstrated the feasibility of examining spinal and nonspinal sources with respect to tissue metabolism and anatomy. A follow-up study with a larger patient population is needed to validate the clinical impact of the proposed method.

DISCLOSURE

This study was funded in part by General Electric Healthcare. No other potential conflict of interest relevant to this article was reported.

ACKNOWLEDGMENTS

We thank Ma A. Ith for coordinating the patient recruitment process and Dr. Deepak Behera for his initial efforts in setting up the study protocol.

REFERENCES

1. Ropper AH, Zafonte RD. Sciatica. *N Engl J Med.* 2015;372:1240–1248.
2. Mixter WJ, Barr JS. Rupture of the intervertebral disc with involvement of the spinal canal. *N Engl J Med.* 1934;211:210–214.
3. Visser LH, Nijssen PG, Tijssen CC, van Middendorp JJ, Schieving J. Sciatica-like symptoms and the sacroiliac joint: clinical features and differential diagnosis. *Eur Spine J.* 2013;22:1657–1664.

4. Kirschner JS, Foye PM, Cole JL. Piriformis syndrome, diagnosis and treatment. *Muscle Nerve.* 2009;40:10–18.
5. Ergun T, Lakadamyali H. CT and MRI in the evaluation of extraspinal sciatica. *Br J Radiol.* 2010;83:791–803.
6. Koes BW, van Tulder MW, Peul WC. Diagnosis and treatment of sciatica. *BMJ.* 2007;334:1313–1317.
7. van der Windt DA, Simons E, Riphagen II, et al. Physical examination for lumbar radiculopathy due to disc herniation in patients with low-back pain. *Cochrane Database Syst Rev.* 2010(2);CD007431.
8. Lewis AM, Layzer R, Engstrom JW, Barbaro NM, Chin CT. Magnetic resonance neurography in extraspinal sciatica. *Arch Neurol.* 2006;63:1469–1472.
9. Haig AJ, Yamakawa K, Kendall R, Miner J, Parres CM, Harris M. Assessment of the validity of masking in electrodiagnostic research. *Am J Phys Med Rehabil.* 2006;85:475–481.
10. el Barzouhi A, Vleggeert-Lankamp CL, Lycklama à Nijeholt GJ, et al. Magnetic resonance imaging in follow-up assessment of sciatica. *N Engl J Med.* 2013;368: 999–1007.
11. Behera D, Jacobs KE, Behera S, Rosenberg J, Biswal S. ^{18}F-FDG PET/MRI can be used to identify injured peripheral nerves in a model of neuropathic pain. *J Nucl Med.* 2011;52:1308–1312.
12. Biswal S, Behera D, Yoon DH, et al. [^{18}F]FDG PET/MRI of patients with chronic pain alters management: early experience [abstract]. *EJNMMI Phys.* 2015;2(suppl 1):A84.
13. Sekine T, Buck A, Delso G, et al. Evaluation of atlas-based attenuation correction for integrated PET/MR in human brain: application of a head atlas and comparison to true CT-based attenuation correction. *J Nucl Med.* 2016;57:215–220.
14. Wollenweber SD, Ambwani S, Lonn AHR, et al. Comparison of 4-class and continuous fat/water methods for whole-body, MR-based PET attenuation correction. *IEEE Trans Nucl Sci.* 2013;60:3391–3398.
15. Wollenweber SD, Ambwani S, Delso G, et al. Evaluation of an atlas-based PET head attenuation correction using PET/CT and MR patient data. *IEEE Trans Nucl Sci.* 2013;60:3383–3390.
16. Ailianou A, Fitsiori A, Syrogiannopoulou A, et al. Review of the principal extra spinal pathologies causing sciatica and new MRI approaches. *Br J Radiol.* 2012;85:672–681.
17. Shi Y, Zong M, Xu X, et al. Diffusion tensor imaging with quantitative evaluation and fiber tractography of lumbar nerve roots in sciatica. *Eur J Radiol.* 2015;84:690–695.
18. Zhou X, Cipriano P, Kim B, et al. Detection of nociceptive-related metabolic activity in the spinal cord of low back pain patients using ^{18}F-FDG PET/CT. *Scand J Pain.* 2017;15:53–57.